International Journal of Biological Macromolecules 183 (2021) 781–789

Contents lists available at ScienceDirect

International Journal of Biological Macromolecules

journal homepage: http://www.elsevier.com/locate/ijbiomac

Innovative production of lignin nanoparticles using deep eutectic solvents for multifunctional nanocomposites

Tong Luo [a], Chao Wang [a,*], Xingxiang Ji [a], Guihua Yang [a], Jiachuan Chen [a], Chang Geun Yoo [b], Srinivas Janaswamy [c], Gaojin Lyu [a,*]

[a] State Key Laboratory of Biobased Material and Green Papermaking, Qilu University of Technology, Shandong Academy of Sciences, Jinan, Shandong 250353, China
[b] Department of Chemical Engineering, State University of New York College of Environmental Science and Forestry, Syracuse, NY 13210, United States
[c] Department of Dairy and Food Science, South Dakota State University, Brookings, SD 57007, United States

ARTICLE INFO

Article history:
Received 9 March 2021
Received in revised form 29 April 2021
Accepted 2 May 2021
Available online 06 May 2021

Keywords:
Lignin
Nanoparticles
Deep eutectic solvents
Poly(vinyl alcohol)
Nanocomposite

ABSTRACT

A green and simple lignin nanoparticles (LNPs) production strategy was developed using deep eutectic solvents (DES). The LNPs were formed with corncob alkali lignin by sequential DES dissolution and self-assembling process. Uniform size and spherical shape of LNPs were observed by scanning electron microscopy (SEM), transmission electron microscopy (TEM), dynamic light scattering (DLS), zeta potential analyzer and gel permeation chromatography (GPC). Less than 100 nm of LNPs were formed, and these particles were preserved without significant size-increase or precipitation within 30 days. The nanocomposite films prepared by incorporating the LNPs into biodegradable poly(vinyl alcohol) (PVA) matrix display good mechanical properties (tensile strength of 82.5 MPa and breaking strain of 103.3%), excellent UV-blocking (100% shielding of the UV spectrum region), strong hydrophobicity (static contact angle of 117.0°) and relatively high thermal stability (the maximum thermal weight loss temperature increased by 40 °C). Overall, this study not only facilitates the advancement of lignin-based nanotechnology by DES but also paves the way for the PVA polymer composites as potential food and medical packaging materials.

1. Introduction

Lignin is a renewable aromatic polymer, accounting for 10–40 wt% of the plant cell wall, and constitutes a promising bioresource for the production of environmentally friendly polymer composites [1–3]. Industrial lignins are produced as by-products with large volume in pulping industry and cellulosic ethanol process [4–6]; however, most of them are being burned as an energy source to generate heat and electricity [7]. There have been a few studies on high-value applications of the usage of lignin, for instance, the production of bio-additives for multifunctional hydrogels [8,9] or nanostructured anode batteries for energy applications such as batteries, supercapacitors and thermoelectric devices [10–12]. The high-value utilization of industrial lignin is still challenging due to lignin's structural complexity and incompatibility with other polymers [13]. Furthermore, heterogeneous characteristics of industrial lignin, large particle size and poor water dispersibility limit its valorization and widespread utility [14,15]. In order to overcome these technical barriers and expand the high-value utilization of lignin, lignin nanoparticles (LNPs) stand tall among possible methods such as amination, sulfonation and depolymerization [16].

Similar to other natural nanoparticles, LNPs could be distributed evenly in the polymer matrix and interact synergistically with the polymer matrix. Consequently, they could be reinforced in a variety of polymers toward improving mechanical, thermal and UV-absorbing properties even with low filler loadings [17]. LNPs could be prepared through a variety of protocols such as mechanical methods, chemical modification and self-assembling [18–20]. Among them, self-assembling gained much attention due to its low energy consumption and simple operation, and more importantly, the versatility to yield particles of uniform size. It is a solution-based micellization process in which lignin will be dissolved in organic solvents such as tetrahydrofuran, dioxane and dimethyl sulfoxide followed by an assembly in a controlled system through dropwise addition or dialysis. Easy volatilization and high toxicity of these organic solvents coupled with non-recyclable nature warrant alternative protocols [19]. Difficulty in controlling the particle size distribution and stable preservation further limit the mass production. In this regard, developing green and facile methods is critical. Such a quest led to deep eutectic solvents (DES), which indeed gained widespread attention due to their low cost, good stability, low toxicity and biodegradable properties [21]. Choline chloride based DES is one successful example [22]. Structural features of lignin recovered from DES pretreated biomass have also been reported [23,24]; however, the application of DES for the LNPs formation with

* Corresponding authors.
E-mail addresses: chaowang@qlu.edu.cn (C. Wang), gaojinlv@qlu.edu.cn (G. Lyu).

https://doi.org/10.1016/j.ijbiomac.2021.05.005
0141-8130/

industrial lignin has not yet been explored. In this regard, a comprehensive study on the activation modification and nanonization strategies of lignin in DES systems provides a novel platform for value-added applications of industrial lignin and forms the basis of the research reported in this submission.

Herein, a facile and green LNPs production with industrial lignin using different DES systems, including acidic and alkaline systems, has been proposed to form size-controllable and stable LNPs. The particle size, morphology, stability, chemical structure and molecular weight of the LNPs were analyzed by dynamic light scattering (DLS), transmission electron microscopy (TEM), scanning electron microscopy (SEM), nuclear magnetic resonance (NMR) and gel permeation chromatography (GPC). We also assessed the technical feasibility of the multifunctional nanocomposites through casting LNPs/PVA films. The overall performance of the obtained nanocomposites was investigated by UV–visible spectrophotometer, thermogravimetric analyzer, mechanical testing instrument and static contact angle tester. The interactions between LNPs and PVA matrix were observed by Fourier transform infrared (FTIR) spectroscopy and SEM. The outcomes from the novel DES approach show the great potentials of the produced LNPs in its food and medical packaging applications.

2. Materials and methods

2.1. Materials

The corncob alkali lignin was obtained from Longlive, Bio-Technology Co., Ltd. (Yucheng, China), which is composed of 6.3% acid soluble lignin, 91.7% acid insoluble lignin and 0.9% ash. The manufacturing and dried process of lignin used in this work was adapted from the previous study [25]. In brief, corncob firstly undergoes dilute acid hydrolysis to produce xylose and meanwhile obtain corncob hydrolysis residue. After further treatment of the residue with alkali, the effluent was separated and adjusted to acidic conditions to precipitate alkali lignin. The lignin was dried under vacuum at 50 °C for 24 h before use. Choline chloride (ChCl) was purchased from Yousuo Chemical Technology Co., Ltd. (Shandong, China). Ethanolamine (ETA), lactic acid (LA) and poly(vinyl alcohol) (PVA) (alcoholysis degree > 99%; M_w = 145 kDa) were purchased from Aladdin Biochemical Technology Co., Ltd. (Shanghai, China). All chemicals used in this study were analytical grade without further purification.

2.2. Synthesis of DES

Deep eutectic solvents were synthesized by our previous work [26]. Briefly, choline chloride (ChCl) and ethanolamine (ETA) were used to synthesize alkaline DES at molar ratios of 1:6. Choline chloride (ChCl) and lactic acid (LA) were used to prepare acidic DES at molar ratios of 1:9.

2.3. Preparation of LNPs

The LNPs dispersion was prepared from corncob alkali lignin in DES by solvent shifting. In brief, a certain amount of lignin was added to DES and stirred for 1 h at ambient temperature (25 °C), then sonicate (240 W) for 20 min to prepare three concentrations of lignin-DES solution (i.e., 1, 3, and 5 wt% in ChCl/ETA or 3 wt% in ChCl/LA). Then, the lignin solution was dialyzed (Spectra/Por® 1 Standard RC Dry Dialysis Tubing, 2 kDa, Spectrum Labs, USA) in deionized water (periodically replaced) for 72 h. The obtained LNPs dispersion was formed and stored in the refrigerator (4 °C) for further characterization and application. Finally, the LNPs were freeze-dried at −50 °C and 0.12 mbar and coded as LNPs-x, where x refers to the initial concentration of lignin solution (1, 3, and 5 wt%).

2.4. Structural characterization of lignin and LNPs

In order to keep the original states of LNPs, the sample was measured without further treatment. The size of LNPs in suspension was detected by DLS, using Zetasizer instrument (Malvern, Nano-ZS90, UK); the suspension was measured three times to obtain exact results. The micro-morphologies of the nanoparticles were observed by SEM (Hitachi Regulus 8220, Japan) at an accelerating voltage of 5 kV. Drops of the LNPs suspension on a silicon substrate, air-dried for 24 h and sputter-coated with gold to provide adequate conductivity. TEM images of the LNPs were obtained by a JEM-2100F TEM under zero-loss conditions at liquid nitrogen temperature. Infrared (IR) spectra of the powdered lignin and LNPs were measured by an FTIR spectrometer (Brooke, ALPHA, Germany). The molecular weight distributions of the samples were determined by GPC according to our previous work [26]. Two-dimensional (2D) heteronuclear single quantum coherence (HSQC) was recorded at room temperature using a Bruker Avance II HD 400 MHz instrument with a BBFO probe equipped with a Z-gradient coil, according to the literature [23,27].

2.5. Preparation and characterization of LNPs/PVA nanocomposite films

The LNPs/PVA nanocomposite films were prepared by a facile solution casting method. First, the PVA was dissolved in deionized water with vigorous stirring at 90 °C for 2 h to prepare a 3 wt% PVA solution. Then, the prepared LNPs-1 suspension and PVA solution were mixed with stirring at 500 rpm for 2 h. After that, the homogeneous mixture of LNPs and PVA was poured onto a plastic mold (90 mm by 90 mm) at once. The composite films with 70 (±10) μm thickness were obtained by evaporating the water and dried at 55 °C for 12 h in a convection oven, then equilibrated for 12 h at a glass desiccator. Four samples with different LNPs contents in the mixture were prepared and labeled as 1%LNPs/PVA, 3%LNPs/PVA, 5%LNPs/PVA and 10%LNPs/PVA, respectively. Parallelly, the control sample, 3%L/PVA, refers to the PVA composites incorporating 3 wt% of corncob alkali lignin, prepared by mixing the aqueous dispersion of the initial form of lignin with PVA solution as evenly as possible. The schematic diagram of the preparation procedure is outlined in Fig. 1a.

For measuring mechanical properties of the films, including tensile strength and elongation at break, dumbbell-shaped samples (75 mm × 4 mm) were tailored according to the standard GB/T1040-2006 at a loading speed of 30 mm min^{-1} at 25 °C under an RH of 50 ± 1% and tested by a texture analyzer (Stable Micro Systems, TA-XTplusC, Germany). Water contact angle (WCA) of the composite films was analyzed by a static contact angle measuring instrument (LAUDA Scientific, LSA100, Japan). The UV-shielding performance and optical transparency of the composite films were determined by a UV–Vis spectrophotometer (Shimadzu, UV 2600, Japan). Thermal performance was performed by thermogravimeter (TA Instruments, Q50, USA), and the heating rate was 10 °C min^{-1} from 50 to 800 °C under N_2 atmosphere according to the literature [28]. Infrared (IR) spectra of the films were measured by an FTIR spectrometer (Brooke, ALPHA, Germany). The morphologies of the obtained films were conducted by SEM (Hitachi Regulus 8220, Japan).

3. Results and discussion

3.1. Particle size, morphology, and stability of the LNPs

The solubility of lignin plays an important role in its commercial applications. The complex structure of lignin could cause its poor solubility and dispersibility in many traditional organic solvents and water. Compared with the commonly used organic solvents like THF, DES showed higher solubility for industrial lignin [29–31]. It was reported that the characteristics of DES affect the applicability of LNPs fabrication

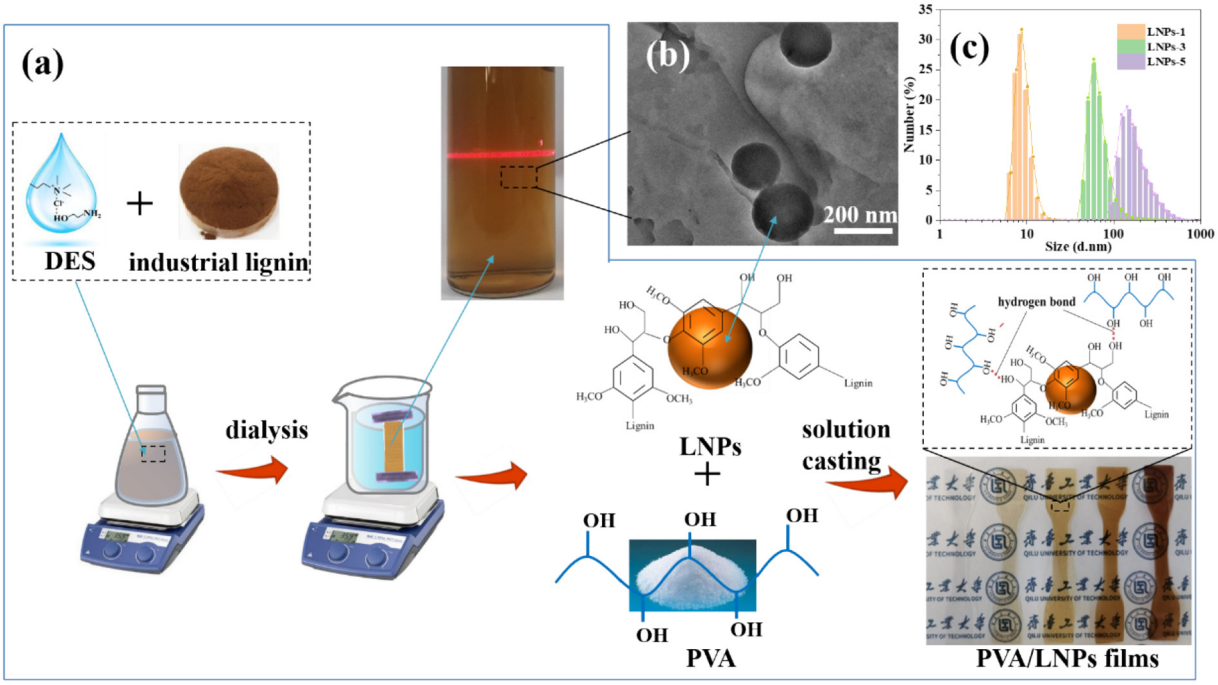

Fig. 1. (a) Schematic representation of the preparation procedure for the LNPs, LNPs/PVA nanocomposite and the hydrogen bond formation mechanism; (b) TEM images of the LNPs-5 and (c) particle size distribution of the LNPs.

methods [24]. In this regard, herein, two different DES were synthesized and tested for the formation mechanism of LNPs.

Herein, the dialysis method was employed to produce LNPs, which exhibited the advantages of simple operation, high applicability, and good spherical productions. As shown in Fig. S1, after dialysis treatment, a better dispersity and stability of LNPs suspension was observed in the alkaline DES system (ChCl/ETA), while the bulk corncob alkali lignin precipitate was formed in the acidic DES system (ChCl/LA). This could be attributed to the polarity of DES. In the solvent exchange process, deionized water enters the acidic solution system and immediately results in lignin precipitation prior to LNPs formation. However, as the alkaline DES were dialyzed out, the solubility of lignin decreased, the hydrophilic units (e.g., hydroxyl and carboxyl functional groups) of lignin extended outward [32]; therefore, the hydrophobic chain segments (phenylpropane structure, etc.) agglomerated inward forming LNPs dispersion [33]. This was similar to the formation of LNPs in the solvent shifting process. The forces for the aggregation of lignin molecules to form nanospheres include hydrophobic interactions, hydrogen bonding, π-interaction, and van der Waals force [18]. Therefore, LNPs obtained in an alkaline system were selected for the further steps.

The particle size, yield, morphology and stability of the LNPs varied depending on the initial concentration of lignin. The yields of LNPs with corncob alkali lignin were presented in Table 1. The values of the yield for LNPs-1, LNPs-3 and LNPs-5 were 70.4, 64.3 and 62.7%, respectively. The particle size distributions and the average size of LNPs were presented in Fig. 1c and Table 1. It was found that the initial lignin concentrations had a significant effect on the final particle diameter. The increase of the initial lignin concentration from 1 to 5 wt% resulted in an increase of the average diameter from 8.9 ± 0.4 nm to 177.0 ± 3.5 nm. This could be attributed to a higher concentration of lignin in the DES system, meaning more lignin is available for the growth of nanoparticles. These variations were further confirmed by TEM (Fig. 1b) and SEM (Fig. 2), it is shown that portray self-assembling of lignin into nanospheres with various morphologies and sizes (Fig. 2b–d) while the initial corncob alkali lignin was irregular in shape with a broad distribution ranging from large micron-sized to nano-sized particles (Fig. 2a). A notable increase in LNPs size accompanied by the increment of inter-particle aggregation was also observed by increasing the lignin concentration.

Table 1
Average size, zeta-potential and yield of the LNPs.

Samples	Average size (d·nm)	Zeta potential (mV)	Yield (wt%)
LNPs-1	8.9 ± 0.4	−30.8 ± 1.0	70.4 ± 2.6
LNPs-3	64.9 ± 2.1	−45.6 ± 1.1	64.3 ± 2.9
LNPs-5	177.0 ± 3.5	−35.8 ± 1.8	62.7 ± 2.1

For better utilization of LNPs in various fields of advanced functional materials, the stability of LNPs dispersion over time is essential [34]. Due to the high content of phenolic hydroxyls and other acidic groups in lignin, the polar groups easily ionize in DES, making LNPs more hydrophilic and soluble. As shown in Table 1, the zeta-potentials of all the LNPs dispersion were higher than −30 mV, indicating relatively high stability of LNPs in anti-solvent (water). The stability of LNPs-3 was further confirmed (Figs. 3 and S2). The LNPs dispersion, quite apparent with light scattering even after 30 days, without significant change in diameter or zeta-potential. The average diameter of LNPs was still ranged from 64.9 to 97.4 nm after 30 days. The excellent stability of LNPs water-dispersion confirms their promising nature with other polymers for nanocomposite fabrication.

3.2. Physicochemical properties of lignin and the LNPs

Further analyses were carried out to investigate the differences in the molecular weight, functional groups, and inter-unit linkages of each LNP. The molecular weights of the lignin and LNPs were listed in Table 2. The weight-average molecular weight (M_w) of the lignin was 3889 Da with a polydispersity index (PDI) of 2.13. After dissolution and dialysis of DES under mild conditions, a subtle increase is noticed in M_w of LNPs range from 4575 and 4657 Da. Thus, the molecular weights were quite stable and are not dependent on the initial lignin concentration. These results suggest the intact molecular weight and PDI of industrial lignin [35,36].

2D-HSQC is an efficient method to further understand the compositional and structural changes of lignin during the LNPs formation. The

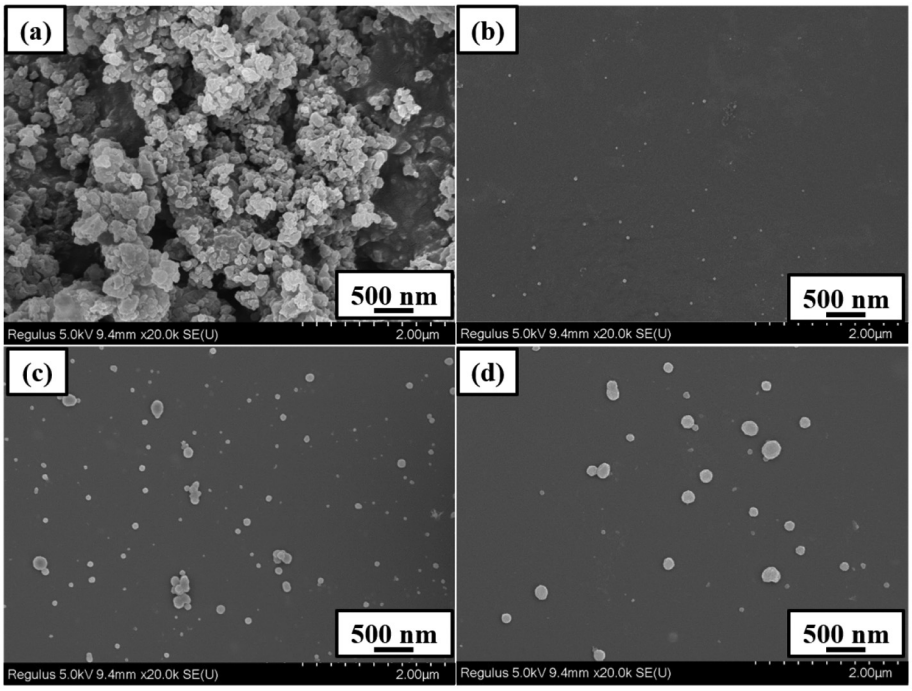

Fig. 2. SEM images of the (a) corncob alkali lignin and LNPs obtained from alkaline DES under different initial concentration. (b) LNPs-1; (c) LNPs-3; (d) LNPs-5.

aliphatic region ($\delta C/\delta_H$ 50.0–90.0/2.50–6.00), aromatic region ($\delta C/\delta_H$ 100.0–150.0/5.50–8.50) and the major substructures are depicted in Fig. 4 [37,38]. In the aliphatic region, the cross-peaks of the inter-unit linkages in lignin and LNPs, such as β-O-4 aryl ether linkages (A) and phenylcoumaran (β-5, C) were the most predominant in all lignin/LNPs fractions, while the resinol, and spirodienone substructures were not detected. The signals for methoxy groups (–OCH_3, $\delta C/\delta_H$ 54.2/3.73) were also noticed. In the aromatic region, the signals of H, S and G units can be clearly seen. Lignin subunits S, G, and H are observed at $\delta C/\delta_H$ 104.8/6.73 ($S_{2,6}$), 111.3/6.90 (G_2), 114.9/6.81 (G_5), 121.6/6.68 (G_6), 129.4/7.01 ($H_{2,6}$), respectively. Additionally, the strong and sharp cross signals at $\delta C/\delta_H$ 112.1/7.33 (FA_2), 131.1/7.32 ($pCA_{2,6}$), 143.5/7.47 (pCA_7) from ferulate (FA) and *p*-coumarate (*p*CA) were detected. Compared with the initial lignin, the G-types in LNPs were decreased, especially the evanescent signal for G_6. It was considered that a large amount of G-type units were connected by A linkage [39]; and the A linkage was relatively easy to be damaged to yield low-molecular weight lignin fractions, which were dialyzed out.

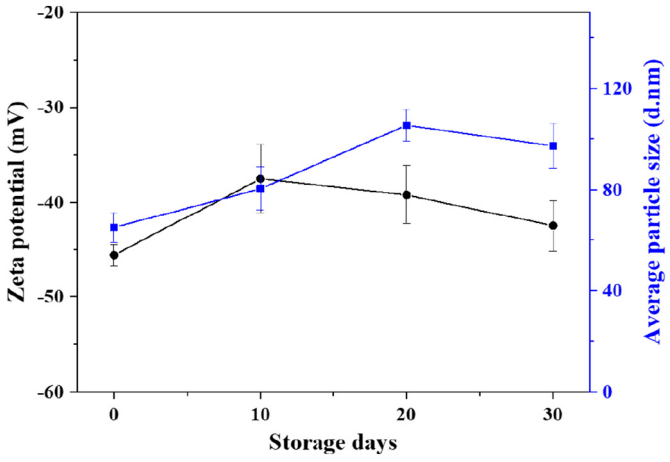

Fig. 3. Average particles size and zeta-potential of the LNPs dispersions for 30 days of storage in refrigerator (4 °C).

3.3. Performance of the LNPs/PVA nanocomposite films

The LNPs-1 was selected for further research, which is expected to well-disperse with the smallest size and good stability for the matrix formation with the PVA. Transparent LNPs/PVA composite films were fabricated by facile solution blending and casting with uniform distribution of LNPs in the PVA matrix. Fig. 5a and Table S1 highlight the stress-strain curves and characteristic mechanical parameters of LNPs/PVA nanocomposites films. Compared with the neat PVA films, the tensile strength of LNPs/PVA nanocomposite enhances significantly, indicating that LNPs addition has a synergistic effect. The hydrogen bonding interactions between PVA and LNPs appear to yield sturdy intermolecular complex and physical crosslinking (Fig. S3) [40]. The tensile strength increased to 63.7 MPa from 46.9 MPa of PVA with only 1 wt% LNPs loading. Furthermore, tensile strength increased with the LNPs amount. For example, when the amount of LNPs increased to 5 wt%, the tensile strength reached 81.0 MPa, which is almost twice that of the neat PVA films. However, further increase of the LNPs content to 10 wt% did not augment the value (82.5 MPa). This could be attributed to the accumulation of larger quantities of LNPs in the PVA matrix [41]. As for the flexibility, the elongation at break of the composite films increased to 110% in 1%LNPs/PVA. A maximum value of 117% in 5%LNPs/PVA was noticed, which is 31% increase compared to 89.0% of the neat PVA. Subsequent decline to 103% with the LNPs addition of 10 wt% was also observed. This may be due to the fact that adding excessive LNPs in the PVA matrix

Table 2
Molecular weights and PDI of pristine lignin and LNPs.

Sample	M_n	M_w	PDI
Corncob alkali lignin	1823	3889	2.13
LNPs-1	2228	4575	2.05
LNPs-3	2295	4657	2.03
LNPs-5	2219	4627	2.08

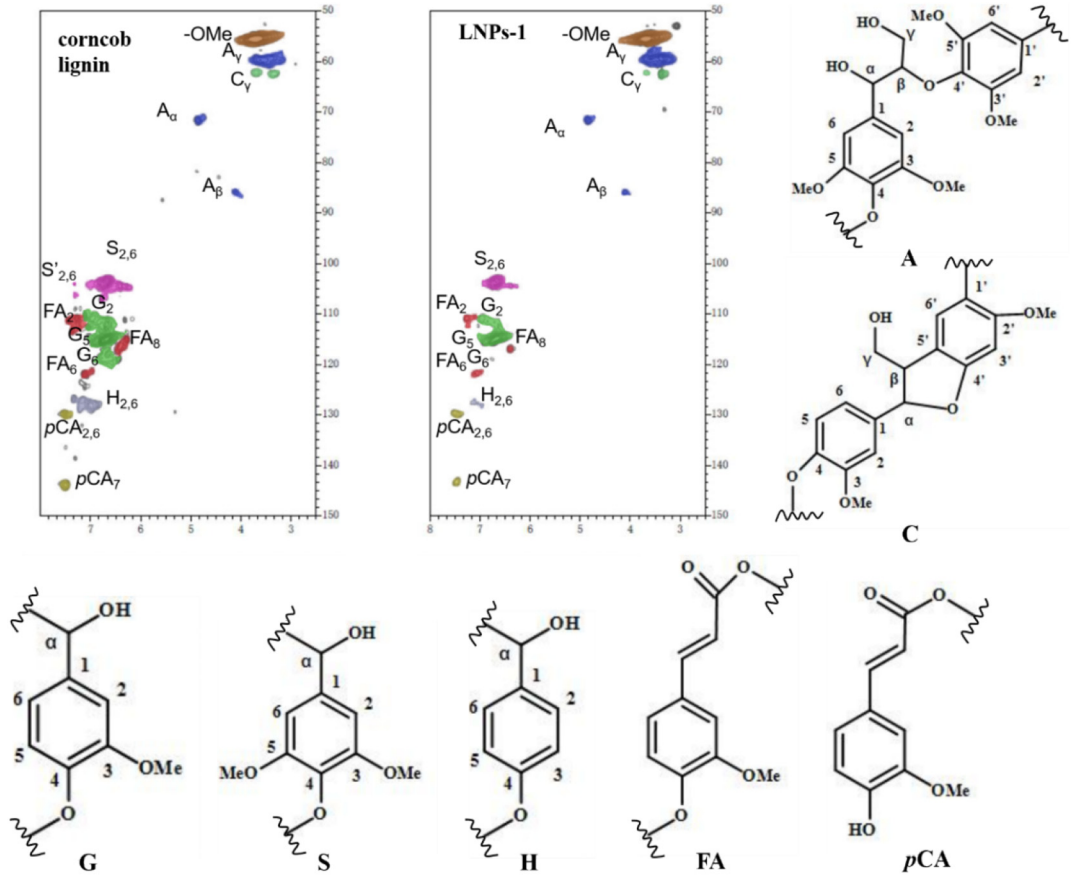

Fig. 4. 2D HSQC NMR spectra of the corncob alkali lignin and LNPs-1. (A) β-O-4 linkages; (C) β-5 linkages; (G) guaiacyl units; (S) syringyl units; (H) *p*-hydroxyphenyl units; (FA) ferulate; (*p*CA) p-coumarate.

could lead to microphase separation in the films that in-turn trigger the elongation with break reduction [42]. The initial form of lignin-water dispersion was directly blended with PVA to produce the film as a control, but the poor interfacial binding between bulk lignin and the polymer matrix usually results in the deterioration of its mechanical performance. As shown by 3%L/PVA, although stress increases to 60.9 MPa, it is still lower than the composite films with the same content of LNPs, and the elongation at break is significantly reduced to 10.3%, which is only about one-ninth of the PVA films. This is could be due to the occurrence of macroscopic phase separation. The nano-effect of LNPs including increased surface area and good dispersion state potentially enhance their compatibility with the PVA matrix; thus, the resulting composite films could exhibit better mechanical performance.

Water contact angle (WCA) measurements were carried out at room temperature, with water droplets 3 μL, under static conditions, and the values were recorded for 30 s. As shown in Fig. 6a, PVA showed a rather high hydrophilicity surface due to the presence of abundant hydroxyl groups on the surface. Compared with the neat PVA films, the WCA of

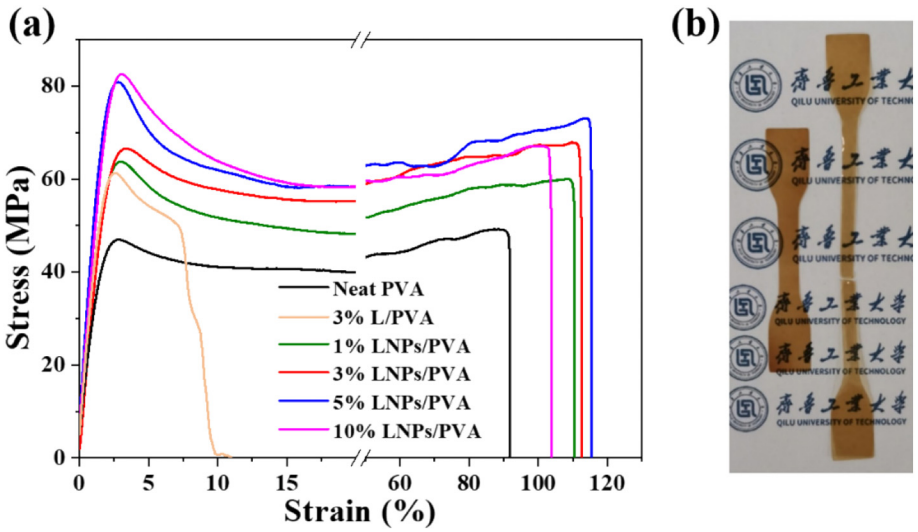

Fig. 5. (a) Stress-strain curves of pure PVA and LNPs/PVA nanocomposite films; (b) photo demonstration of the films 5%LNPs/PVA before and after extension.

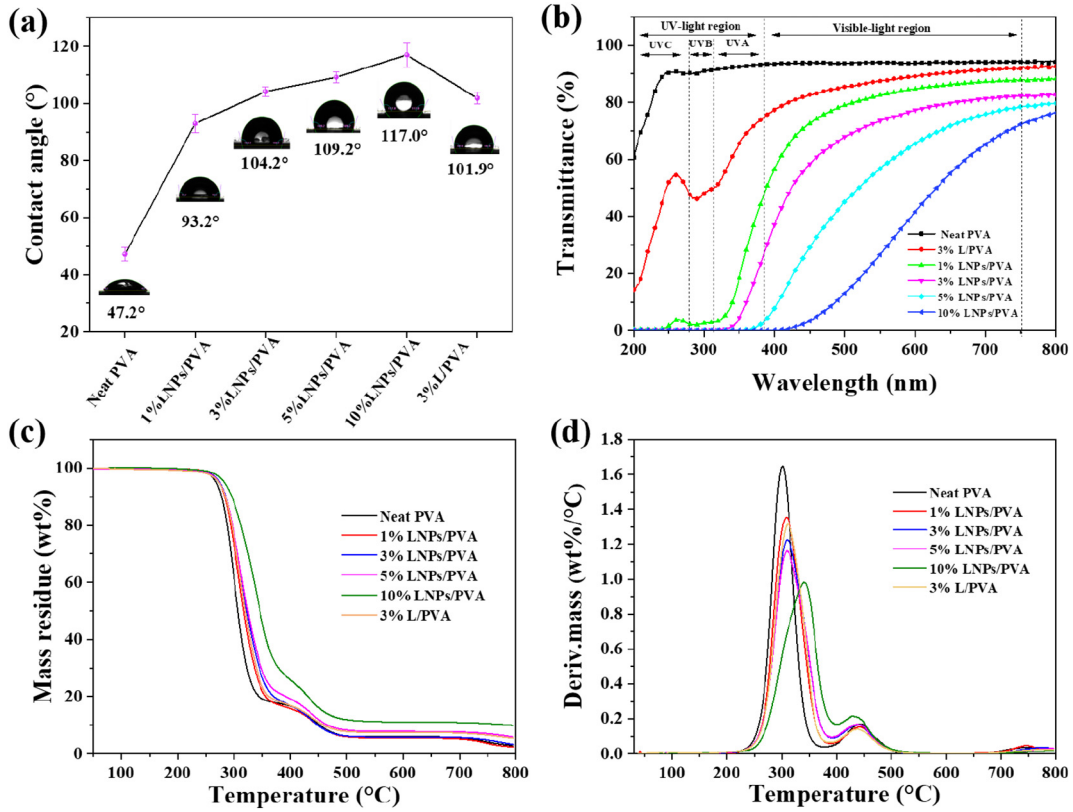

Fig. 6. (a) Static contact angle of pure PVA and LNPs/PVA nanocomposite films; (b) UV–Vis transmittance curves of PVA and LNPs/PVA nanocomposite films; (c) TG and (d) DTG curves of PVA and LNPs/PVA nanocomposite films.

1%LNPs/PVA films increased from 47.2° for PVA to 93.2° with only 1 wt% addition of LNPs, which is preserved up to 10% with a value of 117.0°. The hydrophobicity of LNPs/PVA films significantly improved because of the surface hydrophobicity of LNPs. The control sample (3%L/PVA) also showed good hydrophobic properties (101.9°), probably due to the intrinsic hydrophobicity of the lignin. The WCA values of LNPs/PVA composite films in this study were better than the biopolymer films with metal oxides and other lignin or LNPs [43,44]. This indicates that the PVA cross-linked with LNPs will reduce the water accessibility of PVA, which certainly expands PVA's application in water-based and alcoholic food contact packaging films.

High transparency and strong UV absorption are significant for film application in food and medicine packaging. As shown in Fig. 6b, the PVA films display high transmittance toward UV. However, the LNPs/PVA nanocomposite films were efficient to block the UV light including both the UVA and UVB regions. The light transmittance declines with the LNPs content. This excellent UV blocking performance could be attributed to the aromatic structure and phenolic hydroxyls in LNPs, which showed strong UV absorption capacity [45,46]. Around 3 wt% of LNPs (3%LNPs/PVA) was sufficient to accomplish the 100% shielding of the UVB and UVC. Further LNPs content increase to 10 wt% resulted in the total blockage of the UV-light. The control sample (3%L/PVA) results showed that the blocking efficiency of the LNPs was much higher than that of pristine corncob alkali lignin in the PVA composite films with the same concentration. As shown in Fig. 1, the brown color introduced by LNPs influenced the transmittance of the PVA films in the visible-light region (400–800 nm). Despite this, the nanocomposite films maintained good transparency in the presence of 5 wt% LNPs, indicating that the addition of LNPs to the PVA films could provide an efficient UV block capacity without influencing its visible light transparency, which could be preferred in food and medicinal packaging [40].

The thermal properties of nanocomposite films are also significant indicators for their utilization as packing materials. Thermal properties of prepared PVA nanocomposite films in the presence of different contents of LNPs is presented in Fig. 6c–d, and Table S2. The melting temperature (T_m) of the PVA nanocomposite decreased with the LNPs content than that of the neat PVA films except for 10%LNPs/PVA, and the T_m of 5%LNPs/PVA reduces to 204.2 °C, which was 15.6 °C lower than that of the PVA (219.8 °C). It appears that LNPs thermal degradation starts at relatively low temperature (159.8 °C, Fig. S4). Fig. 6d highlights the DTG curves of the films. The maximum thermal decomposition rate temperature (T_{max}) increased with the LNPs addition, for example, from 300.3 °C of PVA to 341.1 °C of 10%LNPs/PVA, which was 13.9% increase. The aromatic structural units of LNPs also play a significant role in the improvement of thermal stability; however, further research is needed to build on this concept. On the other hand, the T_{max} of the control sample, 3%L/PVA, was 309.2 °C, which was lower than that of 3%LNPs/PVA, and the maximum thermal decomposition rate (0.18 wt%/°C) was also higher than that of the 3%LNPs/PVA. These results confirm that LNPs have good compatibility with PVA and are able to improve the thermal stability of the composite films. These LNPs/PVA nanocomposite films also outperform the lignin nanomicelle/PVA blend [41].

3.4. Interactions between LNPs and PVA matrix

The synergistic interactions between PVA and LNPs were confirmed by the ATR-FTIR (Fig. 7). The PVA exhibited a hydroxyl (O—H) stretching vibration peak at 3270 cm^{-1}. However, with the LNPs loading, a gradual shift to 3254 cm^{-1} was noticed, depending on the LNP concentration. In addition, a similar shift was also evident in C-OH groups vibration, which offset from 1085 to 1082 cm^{-1}. These changes clearly highlight the strong hydrogen bonding interactions between hydroxyl groups in PVA and hydrophilic polar groups (hydroxyl and carboxyl functional groups) in LNPs [17,41].

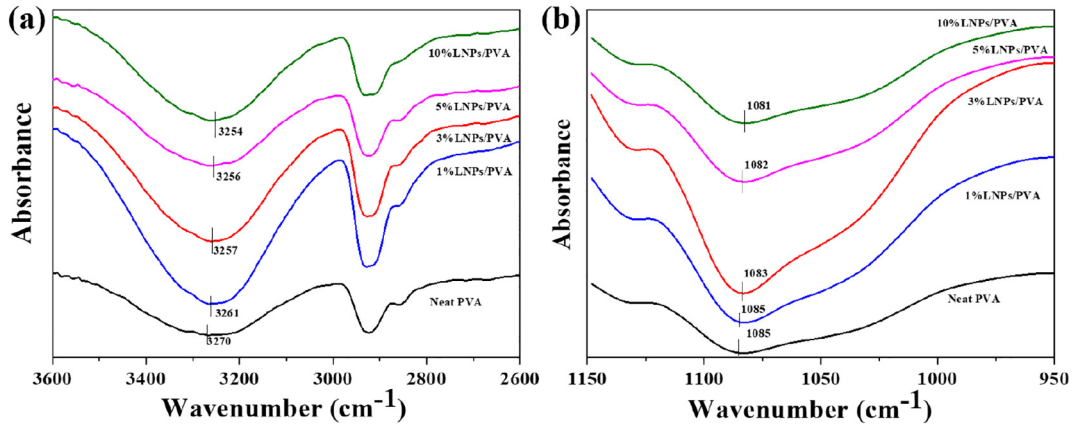

Fig. 7. O—H (a) and C—O (b) stretching vibrations of PVA and LNPs/PVA nanocomposites films.

To reveal the enhanced mechanism of LNPs/PVA nanocomposite films, the dispersion of LNPs in the PVA matrix was studied by SEM. As shown in Fig. 8, PVA exhibits a flat and uniform surface, and LNPs were dispersed without aggregation. The morphological structure of the LNPs was slightly changed after incorporation into the PVA matrix but still preserving their nanoscale structure. On the other hand, the surface of the control group 3%L/PVA showed agglomeration of micron-sized lignin particles. The presence of LNPs in the PVA matrix to form a microscopic phase separation structure greatly increases the hydrophobic group of the nanocomposite films and ultimately leads to an increase in the contact angle. These strong interactions may also be the driving forces to improve the mechanical properties of the nanocomposite films. In addition, the good dispersion state of LNPs was responsible for the excellent UV shielding and thermodynamics performance of the films [41].

4. Conclusions

The LNPs with the preservation of structural integrity of the original lignin were fabricated by an eco-friendly and economic process in the lignin-DES system without catalysts, toxic organic reagents and any other chemical modification steps. The alkaline DES system formed a smaller size (10–200 nm) and good dispersibility of the LNPs with stability over 30 days without significant changes in diameter and zeta-potential. Lignin nanoparticle was chosen as a good candidate for the next-generation functional nanocomposite films. Compared with the pure PVA films, the addition of LNPs improved the mechanical behavior of the LNPs/PVA nanocomposite films, and the tensile strength reached a maximum of 82.5 MPa at 10% LNPs addition which is nearly twice that of the PVA films. The incorporation of 3 wt% LNPs could achieve the full shielding of UVB and UVC and the majority of UVA shielding. The hydrophobicity and thermal stability of the nanocomposite films were also enhanced by introducing the LNPs. Overall, this study proposes a new solvent system to transform the industrial lignin into nanoparticles by an eco-friendly method. It further shows a significant means to prepare fully biodegradable and highly hydrophobicity PVA materials with excellent mechanical performance for a variety of applications such as food and medical packaging materials with UV-blocking behavior.

CRediT authorship contribution statement

Tong Luo: Data curation, Writing-Original draft preparation. Chao Wang: Conceptualization, Methodology, Formal analysis. Xingxiang Ji: Resources. Guihua Yang: Resources, Validation. Jiachuan Chen:

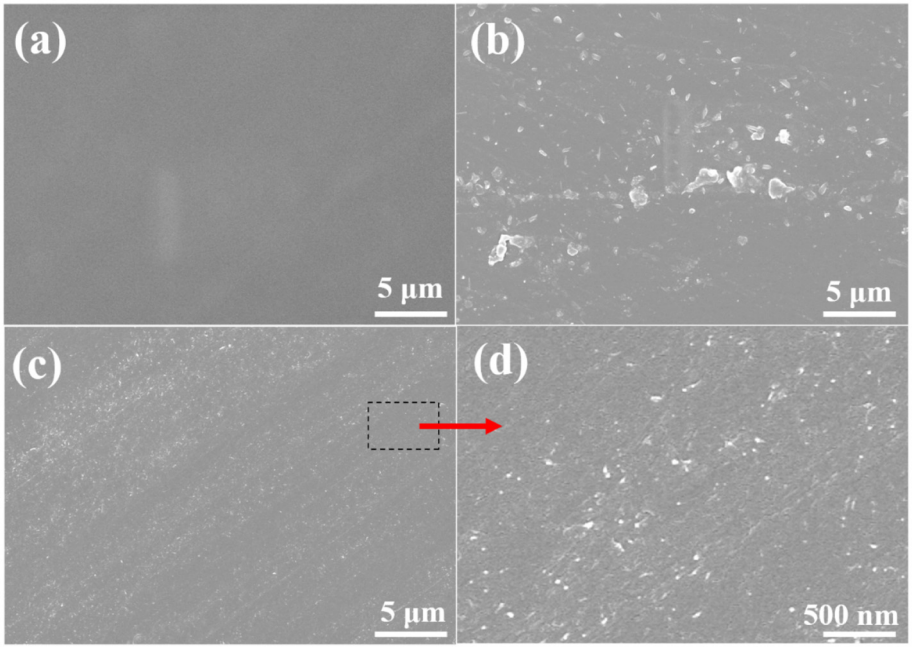

Fig. 8. SEM images of the nanocomposite films. (a) Neat PVA; (b) 3%L/PVA; (c) and (d) 3%LNPs/PVA.

Supervision. Chang Geun Yoo: Formal analysis, Writing-Reviewing and editing. Srinivas Janaswamy: Writing-Reviewing and editing. Gaojin Lyu: Funding acquisition, Project administration, Writing-Reviewing and editing.

Acknowledgments

The authors are grateful for the support of the National Natural Science Foundation of China (Grant No. 31770630; 32001275), China Postdoctoral Science Foundation (Grant No. 2019M652387), Shandong Province Key Research and Development Program of China (No. 2019JZZY010501), Taishan Scholar Project of Shandong Province and USDA National Institute of Food and Agriculture (SD00H648-18).

Appendix A. Supplementary data

Digital images of the LNPs obtained under different types of DES (Fig. S1); Digital images of Tyndall effect of the LNPs dispersions initial state and 30 days later (Fig. S2); Schematic diagram of the hydrogen bond formation mechanism (Fig. S3); TG and DTG curves of corncob alkali lignin and LNPs (Fig. S4); Polarized light microscopy images of different amounts of lignin dissolved in two DESs (Fig. S5); Bulk density images of LNPs-1 and corncob alkali lignin (Fig. S6); N_2 adsorption-desorption isotherms of LNPs-1 (Fig. S7); FTIR spectra of deionized water and DES before and after dialysis (Fig. S8); Characteristic mechanical parameters of LNPs/PVA films (Table S1); Thermal characters of PVA and LNPs/PVA films obtained from DSC and TG tests (Table S2); Specific surface areas of LNPs (Table S3); Compared the conductivity of deionized water and DES before and after dialysis (Table S4). Supplementary data to this article can be found online at https://doi.org/10.1016/j.ijbiomac.2021.05.005.

References

[1] A.J. Ragauskas, G.T. Beckham, M.J. Biddy, R. Chandra, F. Chen, M.F. Davis, B.H. Davison, R.A. Dixon, P. Gilna, M. Keller, P. Langan, A.K. Naskar, J.N. Saddler, T.J. Tschaplinski, G.A. Tuskan, C.E. Wyman, Lignin valorization: improving lignin processing in the biorefinery, Science 344 (2014), 1246843, https://doi.org/10.1126/science.1246843.

[2] B.M. Upton, A.M. Kasko, Strategies for the conversion of lignin to high-value polymeric materials: review and perspective, Chem. Rev. 116 (2016) 2275–2306, https://doi.org/10.1021/acs.chemrev.5b00345.

[3] J. Rajesh Banu, S. Kavitha, R. Yukesh Kannah, T. Poornima Devi, M. Gunasekaran, S.H. Kim, G. Kumar, A review on biopolymer production via lignin valorization, Bioresour. Technol. 290 (2019), 121790, https://doi.org/10.1016/j.biortech.2019.121790.

[4] Z. Sun, B. Fridrich, A. de Santi, S. Elangovan, K. Barta, Bright side of lignin depolymerization: toward new platform chemicals, Chem. Rev. 118 (2018) 614–678, https://doi.org/10.1021/acs.chemrev.7b00588.

[5] C. Somerville, H. Youngs, C. Taylor, S.C. Davis, S.P. Long, Feedstocks for lignocellulosic biofuels, Science 329 (2010) 790–792, https://doi.org/10.1126/science.1189268.

[6] H. Li, Y. Deng, B. Liu, Y. Ren, J. Liang, Y. Qian, X. Qiu, C. Li, D. Zheng, Preparation of nanocapsules via the self-assembly of kraft lignin: a totally green process with renewable resources, ACS Sustain. Chem. Eng. 4 (2016) 1946–1953, https://doi.org/10.1021/acssuschemeng.5b01066.

[7] H. Luo, M.M. Abu-Omar, Chemicals from lignin, Encyclopedia of Sustainable Technologies 2017, pp. 573–585, https://doi.org/10.1016/B978-0-12-409548-9.10235-0.

[8] M. Culebras, A. Barrett, M. Pishnamazi, G.M. Walker, M.N. Collins, Wood-derived hydrogels as a platform for drug-release systems, ACS Sustain. Chem. Eng. 9 (2021) 2515–2522, https://doi.org/10.1021/acssuschemeng.0c08022.

[9] C. Gao, L. Xiao, J. Zhou, H. Wang, S. Zhai, Q. An, Immobilization of nanosilver onto glycine modified lignin hydrogel composites for highly efficient p-nitrophenol hydrogenation, Chem. Eng. J. 403 (2021)https://doi.org/10.1016/j.cej.2020.126370.

[10] T. Akiba, A. Tsurumaki, H. Ohno, Induction of lignin solubility for a series of polar ionic liquids by the addition of a small amount of water, Green Chem. 19 (2017) 2260–2265, https://doi.org/10.1039/c7gc00626h.

[11] M. Culebras, M. Pishnamazi, G.M. Walker, M.N. Collins, Facile tailoring of structures for controlled release of paracetamol from sustainable lignin derived platforms, Molecules 26 (2021)https://doi.org/10.3390/molecules26061593.

[12] M. Culebras, G. Ren, S. O'Connell, J.J. Vilatela, M.N. Collins, Lignin doped carbon nanotube yarns for improved thermoelectric efficiency, Adv. Sustain. Syst. 4 (2020) https://doi.org/10.1002/adsu.202000147.

[13] A. Eraghi Kazzaz, P. Fatehi, Technical lignin and its potential modification routes: a mini-review, Ind. Crop. Prod. 154 (2020), 112732, https://doi.org/10.1016/j.indcrop.2020.112732.

[14] R. Sun, Across the board: Runcang Sun on lignin nanoparticles, ChemSusChem 13 (2020) 1–4, https://doi.org/10.1002/cssc.202000755.

[15] L. Chen, X. Zhou, Y. Shi, B. Gao, J. Wu, T.B. Kirk, J. Xu, W. Xue, Green synthesis of lignin nanoparticle in aqueous hydrotropic solution toward broadening the window for its processing and application, Chem. Eng. J. 346 (2018) 217–225, https://doi.org/10.1016/j.cej.2018.04.020.

[16] S. Iravani, R.S. Varma, Greener synthesis of lignin nanoparticles and their applications, Green Chem. 22 (2020) 612–636, https://doi.org/10.1039/c9gc02835h.

[17] X. Zhang, W. Liu, D. Yang, X. Qiu, Biomimetic supertough and strong biodegradable polymeric materials with improved thermal properties and excellent UV-blocking performance, Adv. Funct. Mater. 29 (2019), 1806912, https://doi.org/10.1002/adfm.201806912.

[18] F. Xiong, Y. Han, S. Wang, G. Li, T. Qin, Y. Chen, F. Chu, Preparation and formation mechanism of size-controlled lignin nanospheres by self-assembly, Ind. Crop. Prod. 100 (2017) 146–152, https://doi.org/10.1016/j.indcrop.2017.02.025.

[19] S.S. Nair, S. Sharma, Y. Pu, Q. Sun, S. Pan, J.Y. Zhu, Y. Deng, A.J. Ragauskas, High shear homogenization of lignin to nanolignin and thermal stability of nanolignin-polyvinyl alcohol blends, ChemSusChem 7 (2014) 3513–3520, https://doi.org/10.1002/cssc.201402314.

[20] B. Wang, D. Sun, H.-M. Wang, T.-Q. Yuan, R.-C. Sun, Green and facile preparation of regular lignin nanoparticles with high yield and their natural broad-spectrum sunscreens, ACS Sustain. Chem. Eng. 7 (2018) 2658–2666, https://doi.org/10.1021/acssuschemeng.8b05735.

[21] X. Tang, M. Zuo, Z. Li, H. Liu, C. Xiong, X. Zeng, Y. Sun, L. Hu, S. Liu, T. Lei, L. Lin, Green processing of lignocellulosic biomass and its derivatives in deep eutectic solvents, ChemSusChem 10 (2017) 2696–2706, https://doi.org/10.1002/cssc.201700457.

[22] Y. Liu, W. Chen, Q. Xia, B. Guo, Q. Wang, S. Liu, Y. Liu, J. Li, H. Yu, Efficient cleavage of lignin-carbohydrate complexes and ultrafast extraction of lignin oligomers from wood biomass by microwave-assisted treatment with deep eutectic solvent, ChemSusChem 10 (2017) 1692–1700, https://doi.org/10.1002/cssc.201601795.

[23] T. Li, G. Lyu, Y. Liu, R. Lou, L.A. Lucia, G. Yang, J. Chen, H.A.M. Saeed, Deep eutectic solvents (dess) for the isolation of willow lignin (Salix matsudana cv. Zhuliu), Int. J. Mol. Sci. 18 (2017) 2266, https://doi.org/10.3390/ijms18112266.

[24] R. Lou, R. Ma, K.-t. Lin, A. Ahamed, X. Zhang, Facile extraction of wheat straw by deep eutectic solvent (DES) to produce lignin nanoparticles, ACS Sustain. Chem. Eng. 7 (2019) 10248–10256, https://doi.org/10.1021/acssuschemeng.8b05816.

[25] L. Dai, R. Liu, L.Q. Hu, Z.F. Zou, C.L. Si, Lignin nanoparticle as a novel green carrier for the efficient delivery of resveratrol, ACS Sustain. Chem. Eng. 5 (2017) 8241–8249, https://doi.org/10.1021/acssuschemeng.7b01903.

[26] T. Luo, C. Wang, X. Ji, G. Yang, J. Chen, S. Janaswamy, G. Lyu, Preparation and characterization of size-controlled lignin nanoparticles with deep eutectic solvents by nanoprecipitation, Molecules 26 (2021) 218, https://doi.org/10.3390/molecules26010218.

[27] L. Zhong, M. Xu, C. Wang, L. Shao, J. Mao, W. Jiang, X. Ji, G. Yang, J. Chen, G. Lyu, C.G. Yoo, F. Xu, Pretreatment of willow using the alkaline-catalyzed sulfolane/water solution for high-purity and antioxidative lignin production, Int. J. Biol. Macromol. 159 (2020) 287–294, https://doi.org/10.1016/j.ijbiomac.2020.05.074.

[28] G. Lyu, Q. Wu, T. Li, W. Jiang, X. Ji, G. Yang, Thermochemical properties of lignin extracted from willow by deep eutectic solvents (DES), Cellulose 26 (2019) 8501–8511, https://doi.org/10.1007/s10570-019-02489-8.

[29] F.H.B. Sosa, D.O. Abranches, A.M. da Costa Lopes, J.A.P. Coutinho, M.C. da Costa, Kraft lignin solubility and its chemical modification in deep eutectic solvents, ACS Sustain. Chem. Eng. 8 (2020) 18577–18589, https://doi.org/10.1021/acssuschemeng.0c06655.

[30] Q. Liu, X. Zhao, D. Yu, H. Yu, Y. Zhang, Z. Xue, T. Mu, Novel deep eutectic solvents with different functional groups towards highly efficient dissolution of lignin, Green Chem. 21 (2019) 5291–5297, https://doi.org/10.1039/c9gc02306b.

[31] B. Xue, Y. Yang, R. Tang, D. Xue, Y. Sun, X. Li, Efficient dissolution of lignin in novel ternary deep eutectic solvents and its application in polyurethane, Int. J. Biol. Macromol. 164 (2020) 480–488, https://doi.org/10.1016/j.ijbiomac.2020.07.153.

[32] T. Pang, G. Wang, H. Sun, L. Wang, Q. Liu, W. Sui, A.M. Parvez, C. Si, Lignin fractionation for reduced heterogeneity in self-assembly nanosizing: toward targeted preparation of uniform lignin nanoparticles with small size, ACS Sustain. Chem. Eng. 8 (2020) 9174–9183, https://doi.org/10.1021/acssuschemeng.0c02967.

[33] G. Wang, T. Pang, S. Chen, W. Sui, C. Si, Y. Ni, Fabrication of lignin nanospheres by emulsification in a binary γ-valerolactone/glycerol system and their application as a bifunctional reducer and carrier for Pd nanoparticles with enhanced catalytic activity, Green Chem. 22 (2020) 8594–8603, https://doi.org/10.1039/d0gc02424d.

[34] M. Ma, L. Dai, C. Si, L. Hui, Z. Liu, Y. Ni, A facile preparation of super long-term stable lignin nanoparticles from black liquor, ChemSusChem 12 (2019) 5239–5245, https://doi.org/10.1002/cssc.201902287.

[35] M. Yang, X. Zhang, S. Guan, Y. Dou, X. Gao, Preparation of lignin containing cellulose nanofibers and its application in PVA nanocomposite films, Int. J. Biol. Macromol. (2020)https://doi.org/10.1016/j.ijbiomac.2020.05.044.

[36] X. Wang, H. Bian, S. Ni, S. Sun, L. Jiao, H. Dai, BNNS/PVA bilayer composite film with multiple-improved properties by the synergistic actions of cellulose nanofibrils and lignin nanoparticles, Int. J. Biol. Macromol. 157 (2020) 259–266, https://doi.org/10.1016/j.ijbiomac.2020.04.178.

[37] X.J. Shen, B. Wang, H.P. li, J.L. Wen, R.C. Sun, Understanding the structural changes and depolymerization of Eucalyptus lignin under mild conditions in aqueous AlCl3, RSC Adv. 6 (2016) 45315–45325, https://doi.org/10.1039/c6ra08945c.

[38] Z. Guo, Q. Zhang, T. You, X. Zhang, F. Xu, Y. Wu, Short-time deep eutectic solvent pretreatment for enhanced enzymatic saccharification and lignin valorization, Green Chem. 21 (2019) 3099–3108, https://doi.org/10.1039/c9gc00704k.
[39] Z. Jiang, H. Zhang, T. He, X. Lv, J. Yi, J. Li, C. Hu, Understanding the cleavage of inter- and intramolecular linkages in corncob residue for utilization of lignin to produce monophenols, Green Chem. 18 (2016) 4109–4115, https://doi.org/10.1039/c6gc00798h.
[40] D. Tian, J. Hu, J. Bao, R.P. Chandra, J.N. Saddler, C. Lu, Lignin valorization: lignin nanoparticles as high-value bio-additive for multifunctional nanocomposites, Biotechnol. Biofuels 10 (2017), 192, https://doi.org/10.1186/s13068-017-0876-z.
[41] X. Zhang, W. Liu, W. Liu, X. Qiu, High performance PVA/lignin nanocomposite films with excellent water vapor barrier and UV-shielding properties, Int. J. Biol. Macromol. 142 (2020) 551–558, https://doi.org/10.1016/j.ijbiomac.2019.09.129.
[42] F. Xiong, Y. Wu, G. Li, Y. Han, F. Chu, Transparent nanocomposite films of lignin nanospheres and poly(vinyl alcohol) for uv-absorbing, Ind. Eng. Chem. Res. 57 (2018) 1207–1212, https://doi.org/10.1021/acs.iecr.7b04108.
[43] J. Wang, Y. Deng, Y. Qian, X. Qiu, Y. Ren, D. Yang, Reduction of lignin color via one-step UV irradiation, Green Chem. 18 (2016) 695–699, https://doi.org/10.1039/c5gc02180d.
[44] S. Gillet, M. Aguedo, L. Petitjean, A.R.C. Morais, A.M. da Costa Lopes, R.M. Łukasik, P.T. Anastas, Lignin transformations for high value applications: towards targeted modifications using green chemistry, Green Chem. 19 (2017) 4200–4233, https://doi.org/10.1039/c7gc01479a.
[45] Y. Wu, Y. Qian, H. Lou, D. Yang, X. Qiu, Enhancing the broad-spectrum adsorption of lignin through methoxyl activation, grafting modification, and reverse self-assembly, ACS Sustain. Chem. Eng. 7 (2019) 15966–15973, https://doi.org/10.1021/acssuschemeng.9b02317.
[46] X. He, F. Luzi, X. Hao, W. Yang, L. Torre, Z. Xiao, Y. Xie, D. Puglia, Thermal, antioxidant and swelling behaviour of transparent polyvinyl (alcohol) films in presence of hydrophobic citric acid-modified lignin nanoparticles, Int. J. Biol. Macromol. 127 (2019) 665–676, https://doi.org/10.1016/j.ijbiomac.2019.01.202.